Journal of Catalysis **192,** 412–422 (2000)
doi:10.1006/jcat.2000.2860, available online at http://www.idealibrary.com on IDEAL®

Physicochemical Characterization of Fe/ZrO_2 Catalysts for NO–CO Reaction

Yasuaki Okamoto,* Takeshi Kubota,* Yoshiharu Ohto,† and Saburo Nasu‡

*Department of Material Science, Shimane University, Matsue 690-8504, Japan; †Department of Chemical Engineering, Faculty of Engineering Science, Toyonaka, Osaka 560-8531, Japan; and ‡Department of Physical Science, Graduate School of Engineering Science, Toyonaka, Osaka 560-8531, Japan
E-mail: yokamoto@riko.shimane-u.ac.jp

Received November 18, 1999; revised February 11, 2000; accepted February 15, 2000

ZrO_2-supported Fe oxide catalysts (Fe/ZrO_2) exhibit a much higher activity in the NO–CO reaction at 523 K than their Al_2O_3- or SiO_2-supported counterparts, in particular at a low Fe content. Physicochemical characterizations of Fe/ZrO_2 with varying Fe loading calcined at 973 K were conducted to disclose the Fe oxide–ZrO_2 interaction modes and the catalytically active species for the NO–CO reaction by means of ^{57}Fe Mössbauer spectroscopy, IR, XRD, XPS, and EXAFS. Three kinds of Fe^{3+} species were shown to be formed; two highly dispersed species and α-Fe_2O_3 particles. Fe^{3+} cation species are preferentially formed below 2.8 Fe nm^{-2} by ion-exchange with the surface OH groups of ZrO_2. After the formation of Fe^{3+} cation species, Fe^{3+} oxide clusters are formed in a maximum amount of 3.4 Fe nm^{-2}. The Fe^{3+} oxide clusters are responsible for the high activity of Fe/ZrO_2, whereas the Fe^{3+} cation species are almost inactive. The addition of Cu improves the activity of Fe/ZrO_2 more than ten times. The catalytic synergy between Fe and Cu is attributed to a cooperative involvement of Cu and Fe. © 2000 Academic Press

Key Words: NO–CO reaction; Fe/ZrO_2; Mössbauer spectroscopy; active species; Fe oxide clusters.

1. INTRODUCTION

The abatement of NO_x from exhaust gases is of great importance for environmental protection (1–8). Nitric oxide reduction by CO is one of the fundamental reactions in the removal of NO from vehicles using precious metals such as Rh, Pt, and Pd (1). Nonprecious metal and metal oxide catalysts were much less extensively explored for the NO–CO reaction than precious metal catalysts, in spite of potential performance at relatively high temperature. Shelef *et al.* (9) reported that the catalytic activity of a metal oxide (10 wt%) supported on Al_2O_3 for the NO–CO reaction decreases in the order $Fe_2O_3 > CuCr_2O_4 > Cu_2O > Cr_2O_3 > NiO > Co_3O_4 > MnO > V_2O_5$. An analogous activity sequence has been confirmed with ZrO_2-supported catalysts in our previous study (10). Moreover, it was found that a ZrO_2-supported Fe oxide catalyst (Fe/ZrO_2) exhibits a much higher activity than Fe oxides supported on SiO_2, Al_2O_3, or SiO_2–Al_2O_3 (10). Recently, Yamaguchi *et al.* (11) found that Cr/ZrO_2 shows activity 20 times higher than Cr/SiO_2 for NO–CO and CO oxidation reactions. ZrO_2-supported Cu oxide catalysts show high activities for these reactions at temperatures as low as 425–470 K, although the activity for the NO–CO reaction rapidly decreases with reaction time, in particular in the initial stage of the reaction (10, 12–14). Perovskite-type mixed oxides, $LaCoO_3$ and La_2CuO_4, have been shown by Mizuno *et al.* (15–17) to disperse very well over the surface of ZrO_2 and to show high activities for the reduction of NO by CO. Thus, ZrO_2-supported Fe, Co, Cr, and Cu oxides show very high catalytic activities for the NO–CO reaction. In addition, it was recently found that SO_4/ZrO_2 systems doped with Fe and Mn are extremely active solid-acid catalysts for the skeletal isomerization of alkanes (18–21). These catalytic features are considered to be a consequence of specific metal oxide–ZrO_2 interactions in these catalyst systems.

The modes of interaction between metal oxides and ZrO_2 have been much less extensively studied (22) up to now than the interaction modes involving Al_2O_3 or SiO_2 as a support. With Fe oxides supported on ZrO_2, the formation of well-dispersed Fe^{3+} oxides at a very low loading of Fe (0.5 wt%) is suggested by XAFS (23). An XAFS study showed that the symmetry of Fe^{3+} species is octahedral (24). Very recently, Fe/ZrO_2 calcined at 723 K was briefly studied by Mössbauer spectroscopy (25, 26). A doublet was tentatively assigned to paramagnetic Fe^{3+} ions at a low loading of Fe (0.8 wt% Fe). Chen *et al.* (26) proposed a vacant surface site model to explain the incorporation of Fe^{3+} cations into the surface layer of ZrO_2. Knowledge of Fe oxide–ZrO_2 surface interactions is very limited in spite of the high feasibility of the ZrO_2-supported Fe oxides as catalysts for the reduction of NO (10) and as promoters of solid-acid catalysts (18–21).

In the present study, Fe/ZrO_2 catalysts with varying Fe-loadings were characterized using ^{57}Fe Mössbauer, IR,

0021-9517/00 $35.00

and XPS spectroscopies and XAFS and XRD techniques. Fe/ZrO_2 catalysts were investigated to obtain fundamental knowledge of catalytic behavior for the NO–CO reaction. It is found that at least three kinds of Fe^{3+} species are formed on the surface of ZrO_2, depending on the loading of Fe. Fe^{3+} oxide clusters are proposed to be responsible for the NO–CO reaction at low temperatures.

2. EXPERIMENTAL

2.1. Catalyst Preparation

Fe/ZrO_2 catalysts were prepared by impregnating ZrO_2 with aqueous solutions of $Fe(NO_3)_3 \cdot 9H_2O$ ($0.8\,cm^3\,g\text{-}ZrO_2^{-1}$). After drying at 383 K for 20 h, the catalyst was calcined in air at 973 K for 1 h using an electric furnace. ZrO_2 was provided by Daiichi-Kigenso Ltd., Japan (EP, BET surface area, 25 $m^2\,g^{-1}$; Hf content, 1.38%) (12–14). A $Cu–Fe/ZrO_2$ catalyst (0.5 wt% Cu and 2 wt% Fe) was prepared by coimpregnation using an aqueous solution containing $Fe(NO_3)_3$ and $Cu(CH_3CO_2)_2$. $Cu–Fe/ZrO_2$ was also calcined at 973 K for 1 h after drying at 383 K for 20 h.

Al_2O_3- and SiO_2-supported Fe catalysts were prepared analogously to the ZrO_2-supported catalysts, for comparison. Al_2O_3 and SiO_2 were provided by the Catalysis Society of Japan as Reference Catalysts (JRC-ALO-4, 177 $m^2\,g^{-1}$, and JRC-SIO-4, 347 $m^2\,g^{-1}$, respectively) (27).

2.2. Reaction Procedure

The NO–CO reaction was carried out using a fixed bed flow reactor made of quartz glass (outer diameter, 6 mmϕ; 0.1 g catalyst) (13, 14). The flow rate of the reaction gas was controlled by means of a mass flow meter (Ueshima-Brooks, 5850E). The concentrations of NO and CO were, respectively, 2500 and 2000 ppm in an He stream (50 $cm^3\,min^{-1}$; W/F, 0.12 g s cm^{-3}, or GHSV, ca. 30,000 h^{-1}). Before the reaction, the catalyst was treated at 673 K for 1 h in a stream of 5% O_2 and cooled to room temperature (RT) in the stream, which was subsequently replaced by an He stream. After complete removal of O_2 in the He stream, the reaction gas containing NO and CO was supplied and the reaction temperature was increased at a rate of 3 K min^{-1} from RT to 523 K. The reaction gas was periodically analyzed by means of an on-line gas chromatograph equipped with columns packed with molecular sieves 5A (NO, CO, N_2, and O_2) and Porapack Q (CO_2 and N_2O).

2.3. Characterization

Mössbauer spectroscopy. The ^{57}Fe Mössbauer spectra were measured at 297 K in a constant acceleration mode using an Elron commercial set which consisted of an MFG-2 signal generator, an MVT-2 velocity transducer, and an MD-2 amplifier (28). Spectra were stored using a multichannel analyzer in a multiscaler mode. Every spectrum was analyzed using a thin foil approximation in which a least-squares fit was carried out assuming Lorentzian absorption lines. The values of the isomer shift are relative to the center position of α-Fe at 300 K. The Mössbauer spectra of 5 wt% Fe/ZrO_2, 10 wt% Fe/Al_2O_3, and 5 wt% Fe/SiO_2 were also measured at 78 K.

X-ray photoelectron spectroscopy (XPS). The X-ray photoelectron spectra of Fe/ZrO_2, Fe/Al_2O_3, and Fe/SiO_2 were accumulated on a Hitachi 507 photoelectron spectrometer using $AlK\alpha_{1,2}$ radiation (1486.6 eV, 450 W). The catalyst sample was mounted on double adhesive tape, followed by evacuation at RT in a pretreatment chamber ($<1 \times 10^{-3}$ Torr). The binding energies for Fe/ZrO_2 were corrected using the Zr 3*d* peak of the ZrO_2 support at 182.2 eV as an internal reference. The binding energy of the Zr 3*d* level had been calibrated using the C 1*s* peak at 285.0 eV due to adventitious carbon. The peak area intensity was calculated assuming a linear background. The binding energy for Fe/Al_2O_3 was referenced to the Al 2*p* level at 74.0 eV.

X-ray absorption fine structure (XAFS). The XAFS spectra of the Fe*K*-edge for the supported Fe catalysts and an α-Fe_2O_3 reference were measured at RT using a Si(111) double-crystal ($d = 0.31366$ nm) monochromator at the BL-6B or 7C station at KEK-PF with 2.5 GeV ring energy and 250–290 mA stored current. In order to eliminate the effects of high-frequency overtones, the beam intensity was detuned to ca. 60%.

The experimental EXAFS spectra were analyzed using a computer program supplied by Technos Co. Ltd. (Japan). Background below the edge jump was subtracted using a Victoreen polynominal with an added constant through the preedge region. Background above the EXAFS region was determined by fitting with a cubic spline. The EXAFS data were analyzed using the FEFF codes (version 6.0) developed by Rehr *et al.* (29). The theoretical phase shifts and backscattering amplitudes were calculated for simple absorber (Fe)–backscatterer (O, Fe, Al, Si) pairs. A spherical wave approximation was used in the calculations using the theoretical EXAFS parameters thus obtained.

Infrared spectroscopy (IR) and X-ray diffraction (XRD). The IR spectra of Fe/ZrO_2 were measured using an *in situ* cell at RT on a Hitachi EPI-G spectrophotometer. The catalyst sample was pressed into a self-supporting disc (45–75 mg/20 mmϕ). The catalyst wafer was evacuated (ca. 10^{-5} Torr) at 573 K for 1 h and subsequently treated with 20 Torr of O_2 for 20 min at the same temperature, followed by degassing for 1 min.

X-ray powder diffraction (XRD) patterns of Fe/ZrO_2 were measured on a Shimazu VD-1 apparatus. The scan speed was $1^\circ\,min^{-1}$.

3. RESULTS

3.1. Catalytic Behavior of Fe/ZrO_2 for the NO–CO Reaction

Figure 1 compares steady-state NO conversions for the NO–CO reaction at 523 K over ZrO_2-, Al_2O_3-, and SiO_2-supported Fe oxide catalysts calcined at 973 K as a function of Fe loading. A relatively high calcination temperature was employed to meet practical applications of the catalysts. The catalysts showed no activity deterioration during the reaction at 523 K even after 50 h. The activity and selectivity were measured after about 20 h on stream. It should be noted that because of the excess amount of NO, the highest NO conversion attainable in the present study is 80% as long as direct decomposition of NO to N_2 and/or N_2O does not take place. No direct decomposition of NO was observed even at 773 K.

Fe/ZrO_2 shows a maximum activity at 5 wt% Fe. The selectivity to N_2 is summarized in Table 1 for the NO–CO reaction at 523 K over Fe/ZrO_2. The maximum selectivity to N_2, 94%, is obtained also for 5 wt% Fe/ZrO_2. With 5 wt% Fe/ZrO_2, it was found that only 40% of reacted NO was converted to N_2 at 473 K, while NO was selectively transformed to N_2 at >543 K. The catalytic activity of Fe/Al_2O_3 is very low at 5 wt% Fe as shown in Fig. 1. It steeply increases and reaches a plateau at 10 wt% Fe. The activity of Fe/SiO_2 is extremely low, but increases in proportion to the Fe content. Fe/ZrO_2 shows a significantly higher activity for the NO–CO reaction than Fe/Al_2O_3 or Fe/SiO_2, in particular at a low Fe loading.

The turnover frequency (TOF) based on the number of Fe atoms, (mole of NO converted) s^{-1} (mole of Fe atoms)$^{-1}$, was calculated for Fe/ZrO_2 and is shown in Fig. 2 as a function of Fe loading. The maximum TOF is observed at 1 wt% Fe; TOF gradually decreases as the Fe content increases above 1 wt%. The TOF value is significantly small for 0.5 wt% Fe/ZrO_2. The dependency of TOF on the Fe loading apparently suggests the formation of several Fe interaction species having different intrinsic activities for the reaction.

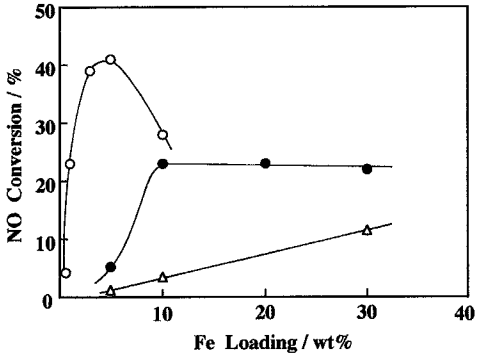

FIG. 1. NO conversions (%) in the NO–CO reaction at 523 K over supported Fe catalysts as a function of Fe loading: ○, Fe/ZrO_2; ●, Fe/Al_2O_3; △, Fe/SiO_2. Partial pressures of NO and CO are 2500 and 2000 ppm, respectively.

TABLE 1

Catalytic Activity of Fe/ZrO_2 at 523 K for the NO–CO Reaction

Fe content (wt%)	NO conversion[a] (%)	Selectivity to N_2[a] (%)	k_{NO}[b]
0.5	4.2	2.2	0.04
1	23	60	3.5
2	37	80	9.5
2[c]	69	100	101
3	39	90	14
5	41	94	16
10	28	36	5.9
0.5 wt% Cu[d]	19	98	2.7

[a] Total flow rate, 50 cm^3 min^{-1}; P_{NO} = 2500 ppm and P_{CO} = 2000 ppm; selectivity to N_2 = (mol of N_2)/[(mol of N_2) + (mol of N_2O)].
[b] 10^{-7} mol s^{-1} g-cat^{-1} $Pa^{-0.5}$ for Fe/ZrO_2.
[c] 0.5 wt% Cu–2 wt% Fe/ZrO_2.
[d] 0.5 wt% Cu/ZrO_2.

The partial pressures of NO and CO (P_{NO} and P_{CO}, respectively) were varied in the range 500–3000 ppm to obtain a reaction rate equation. The flow rate was increased to 100 cm^3 min^{-1} so that the conversions of NO and CO were kept low (<20%). The reaction rate over Fe/ZrO_2 at 523 K could be described by the following rate equation:

$$r = k_{NO} P_{NO}^{-0.41} P_{CO}^{0.91}. \quad [1]$$

The rate constant k_{NO} obtained using Eq. [1] is listed in Table 1 for Fe/ZrO_2.

It was shown previously (10, 14) that the addition of a small amount of Fe to Cu/ZrO_2 significantly increases the activity of Cu/ZrO_2 for the NO–CO reaction. In conformity with the previous observations, the addition of 0.5 wt% Cu to 2 wt% Fe/ZrO_2 drastically increases the activity of Fe/ZrO_2. With 0.5 wt% Cu–2 wt% Fe/ZrO_2, NO reacts with CO at a temperature as low as 390 K (463 K for Fe/ZrO_2), producing N_2O as a major product. Nitric oxide is selectively converted to N_2 at 510 K (543 K for Fe/ZrO_2). The

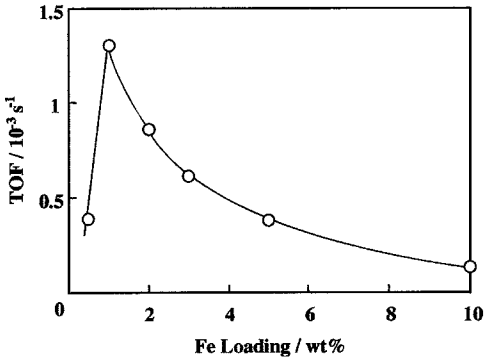

FIG. 2. Turnover frequency (TOF) of Fe species on Fe/ZrO_2 for the NO–CO reaction at 523 K as a function of Fe loading.

rate equation was found to be altered by the addition of Cu and is expressed by Eq. [2] (14):

$$r = k'_{NO} P_{NO}^{0.8} P_{CO}^{0.9}. \quad [2]$$

The rate constants k'_{NO} for Cu–Fe/ZrO_2 and 0.5 wt% Cu/ZrO_2 (14) are presented in Table 1 as well. The rate constant of 2 wt% Fe/ZrO_2 is increased more than 10 times by the addition of 0.5 wt% Cu. Evidently, this activity increase is not due to the activity of the added Cu itself. It is evident that a catalytic synergy is generated between Cu and Fe, as reported previously (14). The activity of Cu–Fe/ZrO_2 was very stable for the NO–CO reaction over 100 h on stream, while that of Cu/ZrO_2 decreased rapidly at a short reaction time, followed by a slow deactivation as shown previously (13).

3.2. *Characterization*

XRD. The XRD patterns of Fe/ZrO_2 are presented in Fig. 3 as a function of Fe content. Only a narrow region of $2\theta = 30°$–$37°$ is presented to clarify the formation of α-Fe_2O_3 (hematite) ((104) at $2\theta = 33.3°$, PDF 01-1053). No formation of other Fe oxide or oxyhydroxide phases was detected by a wide-scan XRD. Fe/ZrO_2 shows a diffraction pattern due to a monoclinic ZrO_2 phase (PDF 36-0420). No diffraction peaks due to Fe oxides are detected below

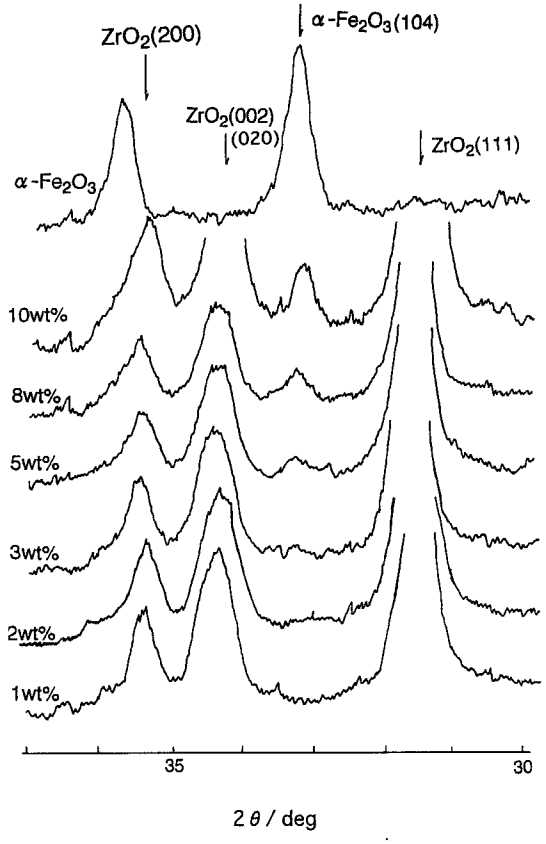

FIG. 3. XRD patterns for Fe/ZrO_2 with varying Fe contents.

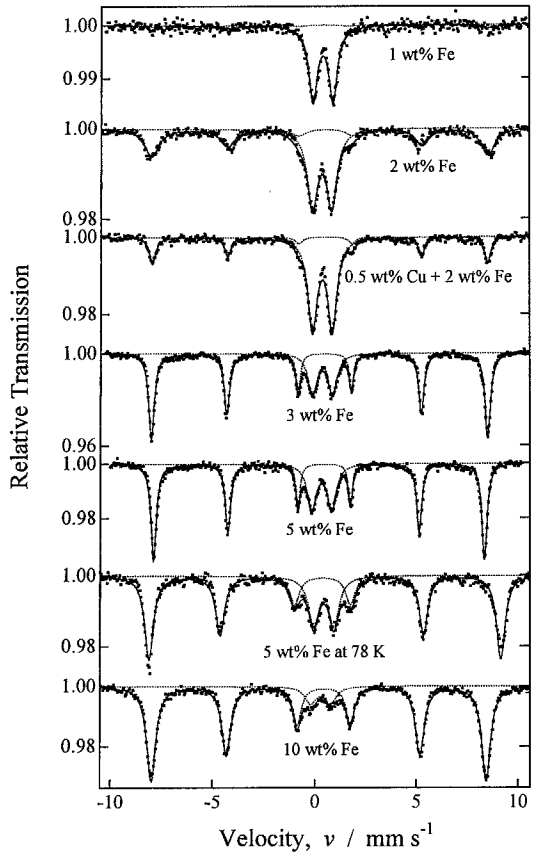

FIG. 4. ^{57}Fe Mössbauer spectra measured at 297 K for Fe/ZrO_2 with varying Fe content. The spectra for 5 wt% Fe/ZrO_2 measured at 78 K and 0.5 wt% Cu + 2 wt% Fe/ZrO_2 are also included.

1 wt% Fe, while a peak at $2\theta = 33.3°$ due to α-Fe_2O_3 grows as the Fe content increases above 2 wt%. This indicates that crystalline α-Fe_2O_3 particles are formed above 2 wt% Fe. The crystallite sizes (D_c) of the ZrO_2 and α-Fe_2O_3 phases were determined from line broadenings using the Scherrer equation (30) (shape factor $K = 0.9$) with the diffraction peaks due to ZrO_2(111) (31.5°) and α-Fe_2O_3(104) (33.3°). The crystallite size of ZrO_2 is 41 nm and is not affected by the addition of Fe. The surface area of the ZrO_2 is estimated from the crystallite size to be 26 $m^2\ g^{-1}$, in excellent agreement with the BET surface area, 25 $m^2\ g^{-1}$. This suggests that the ZrO_2 employed here is composed of crystalline particles without porosity. The size of the α-Fe_2O_3 crystallites increases linearly from 27 to 60 nm as the Fe content increases from 2 to 10 wt%: 27, 30, 40, and 60 nm for 2, 3, 5, and 10 wt% Fe/ZrO_2, respectively.

The XRD pattern of 10 wt% Fe/SiO_2 showed no diffraction peaks due to a crystalline phase except for a very weak peak at $2\theta = 33.3°$ probably due to α-Fe_2O_3. On the other hand, 20 wt% Fe/Al_2O_3 showed a weak XRD pattern, clearly indicating the formation of α-Fe_2O_3 particles.

Mössbauer spectroscopy. Shown in Fig. 4 are the room-temperature Mössbauer spectra of Fe/ZrO_2 catalysts

calcined at 973 K for 1 h. The spectra are composed of, at least, two components, a paramagnetic doublet and a magnetically split sextet. The Mössbauer parameters are summarized in Table 2. Comparing the Mössbauer parameters in Table 2 with those reported for Fe catalysts and reference compounds (25, 31–34), the doublet is attributed to highly dispersed Fe^{3+} species, that is, paramagnetic Fe^{3+} ions and/or superparamagnetic Fe^{3+} oxide clusters, while the sextet is unambiguously assigned to large α-Fe_2O_3 particles. The isomer shift (IS) of 0.30–0.36 mm s^{-1} and the quadrupole splitting (ΔEq) value of 0.96–1.03 mm s^{-1} for the doublet component suggest the formation of Fe^{3+} species in a distorted octahedral symmetry, since these values are in between the values (35) reported for Fe^{3+} cations in an octahedral (IS $\sim$ 0.39 mm s^{-1}, $\Delta Eq \sim$ 0.64 mm s^{-1}) and tetrahedral symmetry (IS $\sim$ 0.21, $\Delta Eq \sim$ 1.29).

The fractions of the highly dispersed Fe^{3+} species and α-Fe_2O_3 particles were calculated from the respective spectral areas and are summarized in Table 2. Figure 5 shows the fraction of the highly dispersed Fe^{3+} species as a function of Fe content. More than 80% of the Fe is highly dispersed in 1 wt% Fe/ZrO_2. It is evident that the fraction of highly dispersed Fe^{3+} species decreases as the Fe content increases. The Mössbauer spectrum of 5 wt% Fe/ZrO_2 was also measured at 78 K to obtain some insights into the possible size distribution of superparamagnetic Fe oxide particles. As shown in Fig. 4 and in Table 2, the fraction of the highly dispersed Fe^{3+} species is essentially unchanged even by the low temperature measurement, showing that with 5 wt% Fe/ZrO_2, there are no superparamagnetic species which transform to magnetically ordered species at 78 K.

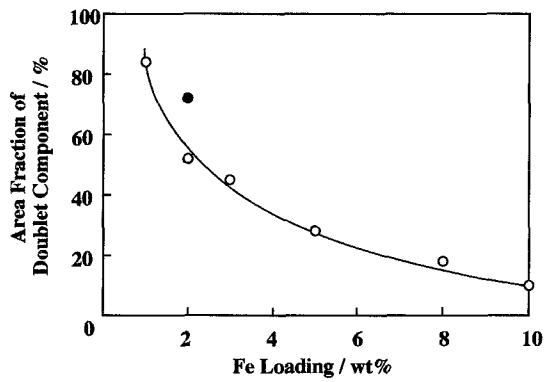

FIG. 5. Area fraction of the doublet component or highly dispersed Fe^{3+} species for Fe/ZrO_2 as a function of Fe loading.

Shown in Fig. 6 are the amounts of the highly dispersed paramagnetic Fe^{3+} species and magnetic α-Fe_2O_3 particles in Fe/ZrO_2 as a function of Fe content. The amount of highly dispersed Fe^{3+} species increases as the Fe content increases and reaches a plateau of 1.4 wt% Fe above 5 wt% Fe. On the other hand, the amount of α-Fe_2O_3 particles increases almost linearly above 1 wt% Fe with increasing Fe content. The latter observations are consistent with the XRD results in Fig. 3 showing a growing peak intensity at 33.3° due to α-Fe_2O_3 crystallites with the Fe content above 2 wt%.

TABLE 2

Mössbauer Parameters for Supported Iron Oxide Catalysts Measured at 297 K

		Doublet			Sextet			
Catalyst[a]	Fe (wt%)	I (%)	IS (mm s^{-1})	ΔEq (mm s^{-1})	I (%)	IS (mm s^{-1})	$\Delta E'q$ (mm s^{-1})	H_i (kOe)
Fe/ZrO_2	1	84	0.34	0.98	16	0.57	−0.18	495
	2	52	0.32	0.96	48	0.26	−0.23	520
	2[b]	72	0.34	0.96	28	0.38	−0.21	512
	3	45	0.33	1.03	55	0.28	−0.19	510
	5	28	0.34	0.98	72	0.26	−0.21	505
		27	0.36	0.97	73	0.27	−0.20	504
	5[c]	25	0.46	1.00	75	0.48	0.16	537
	8	18	0.33	0.95	82	0.27	−0.21	510
	10	10	0.30	0.98	90	0.26	−0.20	510
Fe/Al_2O_3	5	100	0.30	0.96				
	5[c]	81	0.40	0.99	19	0.48	−0.19	519
	10	100	0.30	0.96				
	10[c]	52	0.40	1.01	48	0.48	−0.15	458
Fe/SiO_2	5	100	0.37	0.77				
	5[c]	60	0.43	0.84	40	0.49	0.00	448
α-Fe_2O_3					100	0.26	−0.21	515

[a] Calcination conditions: 973 K for 1 h.
[b] Cu–Fe/ZrO_2 catalyst having 2 wt% Fe and 0.5 wt% Cu.
[c] Mössbauer spectrum was measured at 78 K.

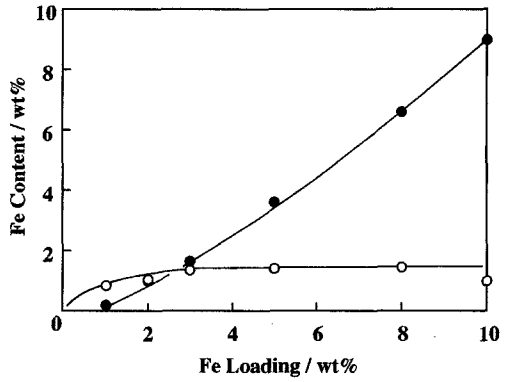

FIG. 6. Amounts of highly dispersed Fe^{3+} species (○) and Fe_2O_3 particles (●) on Fe/ZrO_2 as a function of Fe loading.

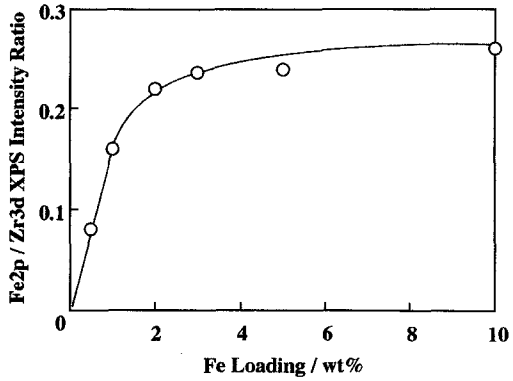

FIG. 8. XPS intensity ratio, Fe 2p/Zr 3d, for Fe/ZrO_2 against the Fe loading.

The effect of Cu addition on the Fe dispersion of 2 wt% Fe/ZrO_2 was studied by Mössbauer spectroscopy as well. As shown in Fig. 4 and Table 2, the spectral contribution of the doublet component is considerably increased by the addition of 0.5 wt% Cu. The amount of highly dispersed Fe^{3+} species is calculated to be 1.4 wt% Fe for Cu–Fe/ZrO_2, close to the maximum amount of the doublet species in Fe/ZrO_2.

The Mössbauer spectra for 10 wt% Fe/Al_2O_3 and 5 wt% Fe/SiO_2 are shown in Fig. 7. The Mössbauer parameters are also presented in Table 2. The spectra are only composed of doublets for Fe/Al_2O_3 as well as Fe/SiO_2 when measured at 300 K. The parameters are close to the values reported for Fe/Al_2O_3 and Fe/SiO_2 with a low Fe content and calcined at a high temperature (32). However, Mössbauer spectra measured at 78 K clearly indicate the formation of sextet species. The Mössbauer parameters demonstrate the formation of small particles of magnetically ordered species different from α-Fe_2O_3 in both catalyst systems, strongly suggesting the formation of binary oxide phases.

XPS. The Fe 2*p* XPS spectra for Fe/ZrO_2 with varying Fe content were measured to obtain information on the chemical states and dispersion of surface Fe species. The Fe $2p_{3/2}$ binding energy was 711.3 ± 0.2 eV irrespective of the Fe content and is characteristic of that for α-Fe_2O_3, indicating the formation of Fe^{3+} oxide species on the Fe/ZrO_2 surface. The XPS intensity ratio, Fe 2*p*/Zr 3*d*, is plotted in Fig. 8 against Fe content. The ratio is proportional to the Fe content up to 1 wt% and becomes more or less constant at a high Fe loading. Taking into consideration theoretical and empirical correlations (36–38) for supported catalysts between the dispersion of surface species and the ratio of the XPS intensities due to the surface species and the support, it is considered from Fig. 8 that Fe^{3+} species are highly dispersed below 1 wt% Fe and that low dispersion species, such as Fe_2O_3 particles, start to form above 1 wt% Fe. The results of XPS are in excellent agreement with those from the XRD and Mössbauer spectroscopy.

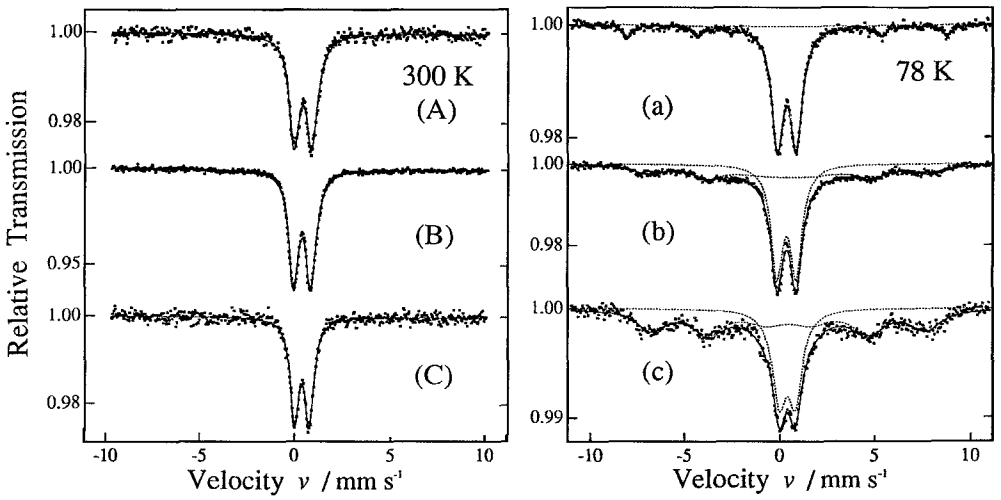

FIG. 7. Mössbauer spectra measured at 300 and 78 K for Fe/Al_2O_3 and Fe/SiO_2 calcined at 973 K for 1 h: (A, a) 5 wt% Fe/Al_2O_3; (B, b) 10 wt% Fe/Al_2O_3; (C, c) 5 wt% Fe/SiO_2.

The Fe $2p_{3/2}$ binding energy for 5 wt% Fe/Al_2O_3 is 711.8 eV, marginally higher than that for Fe_2O_3. With 5 and 10 wt% Fe/SiO_2, the XPS intensity of the Fe $2p$ band was too weak to detect on the present spectrometer, indicating that most of the Fe species are in the bulk of the catalyst.

XAFS. Figures 9 and 10 show the k^3-weighted EXAFS functions and the corresponding Fourier transforms for Fe/ZrO_2, Fe/Al_2O_3, and Fe/SiO_2. The Fourier transform for 5 wt% Fe/ZrO_2 is obviously very close to that for α-Fe_2O_3, suggesting that the local structure of most Fe^{3+} species is similar to that in α-Fe_2O_3. On the other hand, 5 wt% Fe/Al_2O_3 shows two weak peaks at 2.5 and 3.0 Å as the second and third shells, respectively. At a higher Fe loading, the Fourier transform for 20 wt% Fe/Al_2O_3 becomes much closer to that for α-Fe_2O_3, in conformity with the XRD results. With 5 wt% Fe/SiO_2, the Fourier transform is considerably different from that for α-Fe_2O_3.

The EXAFS results on the 5 wt% Fe catalysts were analyzed using theoretical parameters ($\Delta k = 3.5$–12 Å^{-1}). The structural parameters thus estimated are summarized in Table 3. Since α-Fe_2O_3 has three Fe–Fe bondings in a narrow range, 2.90–3.36 Å, as presented in Table 3, it was impossible to reproduce the structural parameters of α-Fe_2O_3 without any restrictions in the curve-fittings. Accordingly, in the case of the EXAFS analysis of the α-Fe_2O_3 reference, the Fe–Fe and Fe–O bond distances were fixed at the corresponding crystallographic values (39) and a theoretical σ value (0.06) was used. The differences in the calculated coordination numbers in Table 3 from the corresponding theoretical values may result from the use of the theoretical parameters and possible contributions of high-frequency overtones in the EXAFS spectra. With 5 wt%

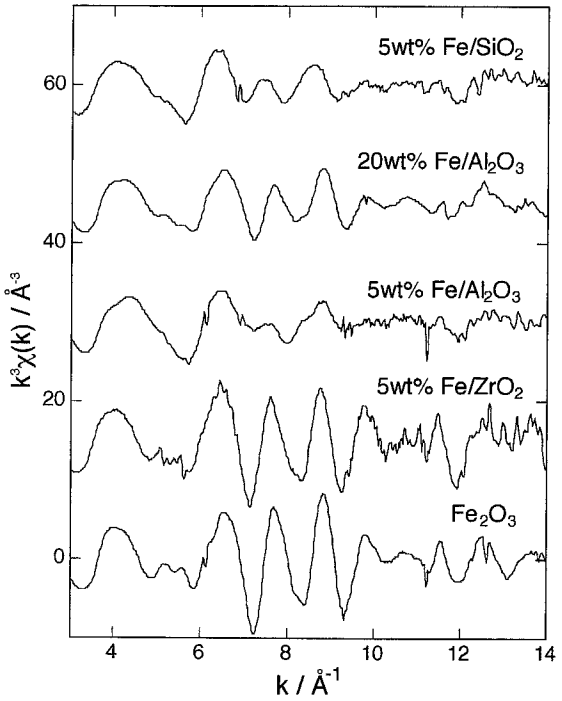

FIG. 9. The k^3-weighted EXAFS functions for supported Fe catalysts and Fe_2O_3.

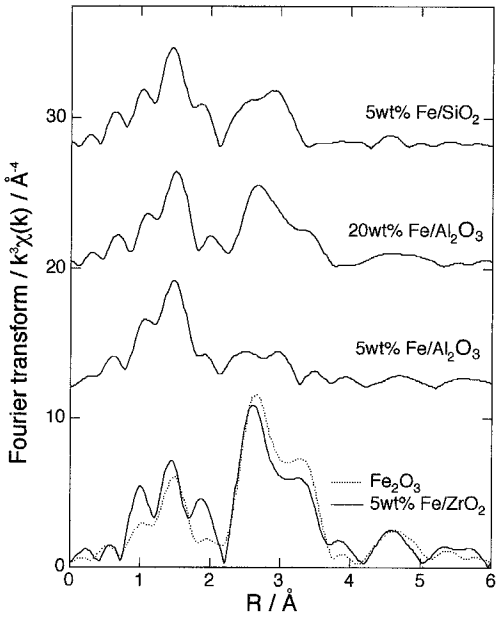

FIG. 10. The k^3-weighted Fourier transforms for supported Fe catalysts and Fe_2O_3 ($\Delta k = 3.5$–12.0 Å).

TABLE 3

Structural Parameters[a] as Derived from the EXAFS Analysis for 5 wt% Fe Catalysts and α-Fe_2O_3

Catalyst	Scatterer	R (Å)	CN[b]	E_0 (eV)	$\Delta\sigma^2$ (Å^2)	R factor (%)
α-Fe_2O_3	O	1.944*	1.8(3)	0.6	0*	18
		2.115*	1.0(3)	5.0	0*	
	Fe	2.897*	1.4(1)	−0.9	0*	34
		2.969*	1.1(3)	−4.7	0*	
		3.360*	2.6(3)	1.6	0*	
Fe/ZrO_2	O	1.944*	1.7	−0.7	0*	39
		2.115*	1.5	9.8	0*	
	Fe	2.897*	1.1	−7.7	0*	27
		2.969*	1.0	−8.7	0*	
		3.360*	2.3	−3.3	0*	
Fe/Al_2O_3	O	1.86	1.5	−3.5	0.0002	7.7
		1.99	1.4	0.5	0.0012	
	Fe	2.93	1.0	−12.2	0.0045	18
	Al	3.33	1.3	7.7	0.0036	
Fe/SiO_2	O	1.88	1.5	−2.4	0.0035	11
		2.00	2.0	−3.5	0.0025	
	Fe	3.06	0.5	0.6	0.0026	1.5
	Si	3.21	2.4	−6.7	0.0056	

[a] An asterisk indicates a fixed parameter; CN, coordination number; R, distance between Fe and scatterer; $\Delta\sigma^2$, relative Debye–Waller factor; R factor is defined as $R = \sum_k (\chi_{fit}(k) - \chi_{exp}(k))^2 / \sum_k \chi_{exp}(k)^2$.

[b] The numbers in parentheses are the crystallographic coordination numbers of α-Fe_2O_3.

Fe/ZrO_2, the formation of α-Fe_2O_3 is assumed and the R and σ-values were fixed at those for α-Fe_2O_3 in the fitting procedures. The coordination numbers of the Fe–O and Fe–Fe bondings for 5 wt% Fe/ZrO_2 thus obtained are very close to the corresponding values obtained for α-Fe_2O_3, confirming that the local structure of the major Fe^{3+} species in 5 wt% Fe/ZrO_2 resembles that in crystalline α-Fe_2O_3. This is in line with the Mössbauer results in Table 2.

With 5 wt% Fe/Al_2O_3 and Fe/SiO_2, the EXAFS results were analyzed without any restrictions. The Fourier transform peaks between 2.1 and 3.3 Å can be reasonably curve-fitted only when Fe–Al or Fe–Si bondings are assumed in addition to Fe–Fe bondings. These results suggest the formation of binary oxides as predominant species in 5 wt% Fe/Al_2O_3 and Fe/SiO_2.

IR. In order to assess the reactivity of the surface hydroxyl groups toward Fe species, IR spectra were measured for Fe/ZrO_2 after evacuation at 623 K. Figure 11 shows the IR spectra of the OH region. As reported previously (12, 13), three kinds of OH groups are observed for the ZrO_2 sample at 3776, 3674, and 3734 cm^{-1}. The former two bands are assigned to terminal and bridged OH groups on ZrO_2 (22, 40), respectively, and the last band is tentatively assigned to the OH groups attached to impurity HfO_2 (12, 13). It is evident that the intensity of the surface OH groups decreases as the Fe content increases. Three kinds of OH groups are almost simultaneously consumed by the incorporation of Fe and are almost completely lost at 5 wt% Fe. The IR peak intensity, which is expressed by log (I_0/I) normalized to the sample weight, of the OH groups at 3776 cm^{-1} is presented in Fig. 12 as a representative of the three bands as a function of Fe loading. It is evident that the OH groups are effectively consumed at 0.5 wt% Fe, followed by a gradual decrease above 1 wt% Fe with increasing Fe loading. These results suggest that the surface OH groups of ZrO_2 are involved in the formation of the highly dispersed Fe^{3+} species.

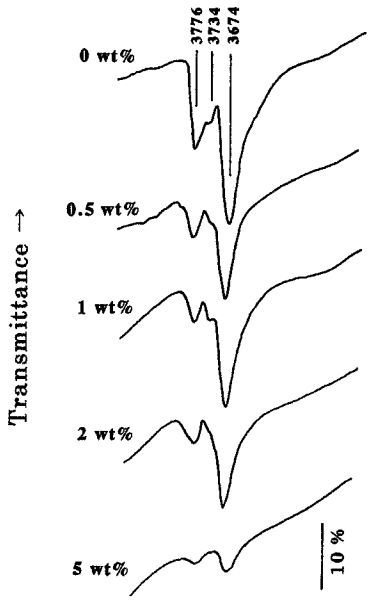

FIG. 11. IR spectra for Fe/ZrO_2 with varying Fe content. Sample weight: 0 wt% Fe, 54.1 mg; 0.5 wt% Fe, 74.5 mg; 1 wt% Fe, 55.7 mg; 2 wt% Fe, 48.7 wt%; 5 wt% Fe, 52.8 mg.

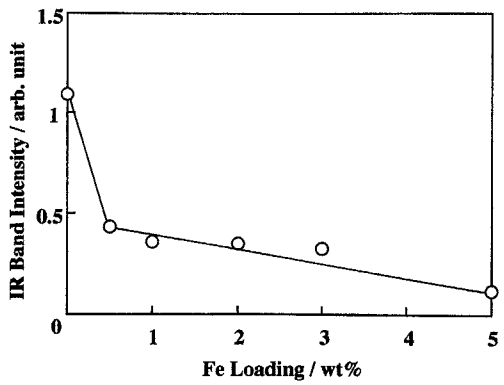

FIG. 12. IR peak intensity, as expressed by log (I_0/I) normalized to the sample weight, of the OH band at 3776 cm^{-1} as a function of Fe loading.

4. DISCUSSION

The XPS results in Fig. 8 on Fe/ZrO_2 evidently indicate that the dispersion of the Fe^{3+} species depends on the Fe loading. In agreement with the XRD observations, highly dispersed Fe^{3+} species are preferentially formed at an Fe content lower than 1 wt%. It is well established (33, 34, 41, 42) that the Mössbauer results for 5 wt% Fe/ZrO_2 measured at 297 and 78 K reflect the particle size distribution of Fe^{3+} species. With 5 wt% Fe/ZrO_2, the area fraction of the doublet component observed at 297 K is essentially unaffected by lowering the measurement temperature within the accuracy of ±5%, indicating that there is no superparamagnetic Fe^{3+} species with a magnetic transition temperature between 78 and 297 K. Consequently, it is concluded that at least two kinds of Fe^{3+} species are formed having different dispersions, highly dispersed Fe^{3+} species showing paramagnetism at 78 K and α-Fe_2O_3 particles large enough to exhibit a magnetically ordered state even at 297 K.

According to Kündig *et al.* (41), the volume V of α-Fe_2O_3 particles is correlated to the transition temperature T where superparamagnetism turns into static magnetic order, by

$$\ln(4 \times 10^{-4} K) = 2KV/kT \qquad [3]$$

where k is the Boltzman constant and K is an anisotropy constant ($4.7 \pm 1.1 \times 10^4$ erg cm^{-3}) experimentally determined for a variety of Fe_2O_3 samples with known particle sizes. The critical diameters of α-Fe_2O_3 particles are

calculated from Eq. [3] to be 13 and 8 nm at 297 and 78 K, respectively. Accordingly, the particle size of the Fe^{3+} species in 5 wt% Fe/ZrO_2, paramagnetic at 78 K, is considerably smaller than 8 nm, even if these species are present as highly dispersed Fe^{3+} oxide clusters. In addition, the particle size of α-Fe_2O_3 is considerably larger than 13 nm. This is in conformity with the XRD results showing the formation of α-Fe_2O_3 crystallites of 40 nm in size. Apparently, a bimodal size distribution of Fe^{3+} species is formed with Fe/ZrO_2 calcined at 973 K, irrespective of the Fe content. In contrast to Fe/ZrO_2, the fraction of the doublet component in Fe/Al_2O_3 or Fe/SiO_2 is considerably decreased by lowering the measurement temperature from 300 to 78 K. Thus, the size distribution of the Fe^{3+} species in Fe/Al_2O_3 and Fe/SiO_2 is broad and different from that in Fe/ZrO_2.

It is important to clarify the catalytically active forms of the Fe^{3+} species in Fe/ZrO_2. The rate constant k_{NO} in Table 1 is plotted in Fig. 13 against the surface area of α-Fe_2O_3, which is calculated on the basis of the crystallite size (XRD) and the amount (Fig. 6) of α-Fe_2O_3. Evidently, no correlation is obtained except for 2 and 3 wt% Fe/ZrO_2.

The rate constant k_{NO} is presented in Fig. 14 as a function of the amount of the highly dispersed Fe^{3+} species (Fig. 6) obtained from the Mössbauer measurements at 297 K. In Fig. 14, the Fe^{3+} species in 0.5 wt% Fe/ZrO_2 are assumed to be fully dispersed on the basis of the correlation in Fig. 5. Evidently, the rate constant is not simply proportional to the amount of Fe species. However, k_{NO} increases linearly with the amount of highly dispersed Fe^{3+} species above 0.65 wt% Fe. On the basis of the correlations shown in Figs. 13 and 14, we are inclined to suggest that some of the highly dispersed Fe^{3+} species bear a major part of the catalytic activity of Fe/ZrO_2 rather than that α-Fe_2O_3 particles show a high activity for the NO–CO reaction.

The intersection value (0.65 wt% Fe) in Fig. 14 suggests that the highly dispersed Fe^{3+} species formed at Fe content below 0.65 wt% are almost inactive. The rate constant

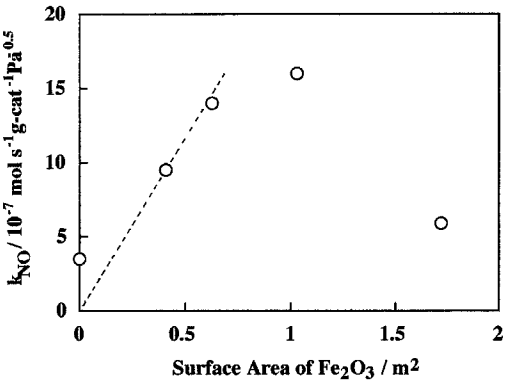

FIG. 13. Rate constant k_{NO} of the NO–CO reaction over Fe/ZrO_2 as a function of the surface area of α-Fe_2O_3 estimated from XRD and Mössbauer results.

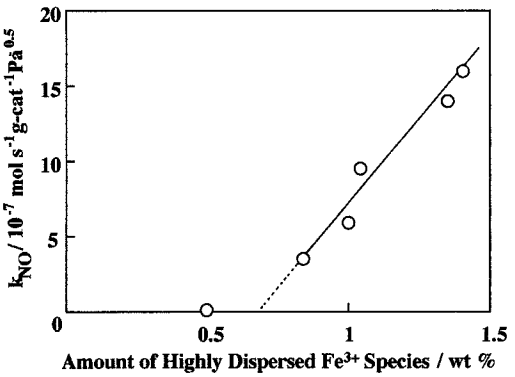

FIG. 14. Correlation between the rate constant k_{NO} of the NO–CO reaction over Fe/ZrO_2 and the amount of highly dispersed Fe^{3+} species calculated from the Mössbauer results at 297 K.

increases linearly with the amount of highly dispersed Fe^{3+} species exceeding 0.65 wt% Fe. The correlation in Fig. 14 obviously suggests the formation of at least two kinds of highly dispersed Fe^{3+} species, catalytically active and inactive species. The latter species are preferentially formed at an Fe loading below 0.65 wt% or 2.8 Fe atoms nm^{-2}. The formation of at least two kinds of highly dispersed Fe^{3+} species is evidenced by the dependence of the surface OH groups on the Fe content (Fig. 12).

As mentioned above, the highly dispersed Fe^{3+} species are ascribed to paramagnetic Fe^{3+} cations or superparamagnetic Fe^{3+} oxide clusters small enough to show paramagnetism at 78 K. Unfortunately, these species cannot be differentiated by the Mössbauer parameters alone. Taking into consideration the correlation shown in Fig. 14, it is tentatively proposed that the catalytically inactive species of 2.8 Fe atoms nm^{-2} are surface paramagnetic Fe^{3+} cations strongly interacting with the surface of ZrO_2. For Fe/ZrO_2 calcined at 723 K (0.8 wt% Fe), Chen *et al.* (26) proposed the formation of analogous paramagnetic Fe^{3+} cations and suggested that these species are trapped in the vacant surface sites of ZrO_2. On the other hand, Yamamoto *et al.* (24) claimed the dissolution of Fe^{3+} cations in the interstitial sites of ZrO_2 for Fe/ZrO_2 calcined at 873 K (1.9 Fe nm^{-2}). The IR results in Fig. 12 indicate that the surface OH groups of ZrO_2 are preferentially consumed at 0.5 wt% Fe, where catalytically inactive species are formed. Accordingly, it is suggested that these Fe^{3+} species are surface Fe^{3+} cation species formed by ion exchange with surface OH groups, resulting in the formation of stable Fe^{3+}–O–Zr^{4+} bonds. The Mössbauer parameters in Table 2 suggest that paramagnetic Fe^{3+} cation species are in a distorted octahedral symmetry, in agreement with the XAFS results reported by Yamamoto *et al.* (24). It is concluded that Fe^{3+} cation species are predominantly formed below 0.65 wt% Fe and that they are too strongly stabilized in the surface sites of ZrO_2 to show catalytic activity for the NO–CO reaction at a reaction temperature as low as 523 K.

A highly dispersed and catalytically active Fe^{3+} species appears above 0.65 wt% Fe. The Mössbauer results indicate that this species is paramagnetic or superparamagnetic in nature. In the latter case, the size of Fe_2O_3 is calculated to be much smaller than 8 nm in diameter. Taking into consideration that the XPS intensity ratio is proportional to the Fe content up to 1 wt% Fe, the catalytically active Fe^{3+} species may be as well spread over the ZrO_2 surface as the Fe^{3+} cation species formed below 0.65 wt% Fe. The IR results in Fig. 12 indicate that only a small number of surface OH groups are consumed in the formation of the active species. Accordingly, it is considered that the catalytically active species are Fe^{3+} oxide clusters produced after the preferential formation of the catalytically inactive Fe^{3+} cation species is complete. The maximum amount of Fe^{3+} oxide clusters is calculated to be 0.8 wt% Fe or 3.4 Fe atoms nm^{-2}. These Fe^{3+} oxide clusters probably interact much less strongly with the surface of ZrO_2 than the Fe^{3+} cation species. Weak interactions between the Fe^{3+} oxide clusters and the surface of ZrO_2 would facilitate easy reduction–oxidation processes during the NO–CO reaction.

The formation of α-Fe_2O_3 particles is observed above 1 wt% Fe by Mössbauer spectroscopy and XRD. The amount and size of the α-Fe_2O_3 particles increase as the Fe content increases. Mössbauer spectroscopy suggests that the diameter of the α-Fe_2O_3 is much larger than 13 nm, in agreement with the XRD results. The saturation in the Fe $2p$/Zr $3d$ XPS intensity ratio is also readily explained in terms of the formation of large Fe_2O_3 particles above 1 wt% Fe (36–38).

It is concluded that at least three kinds of distinctly different Fe^{3+} species, that is, two kinds of highly dispersed Fe^{3+} species and α-Fe_2O_3 particles, are formed on the surface of ZrO_2. The Fe^{3+} oxide clusters interacting weakly with the ZrO_2 surface are responsible for a major part of the catalytic activity at 523 K as shown in Fig. 14. A schematic model of Fe/ZrO_2 calcined at 973 K is shown in Fig. 15 as a function of Fe loading.

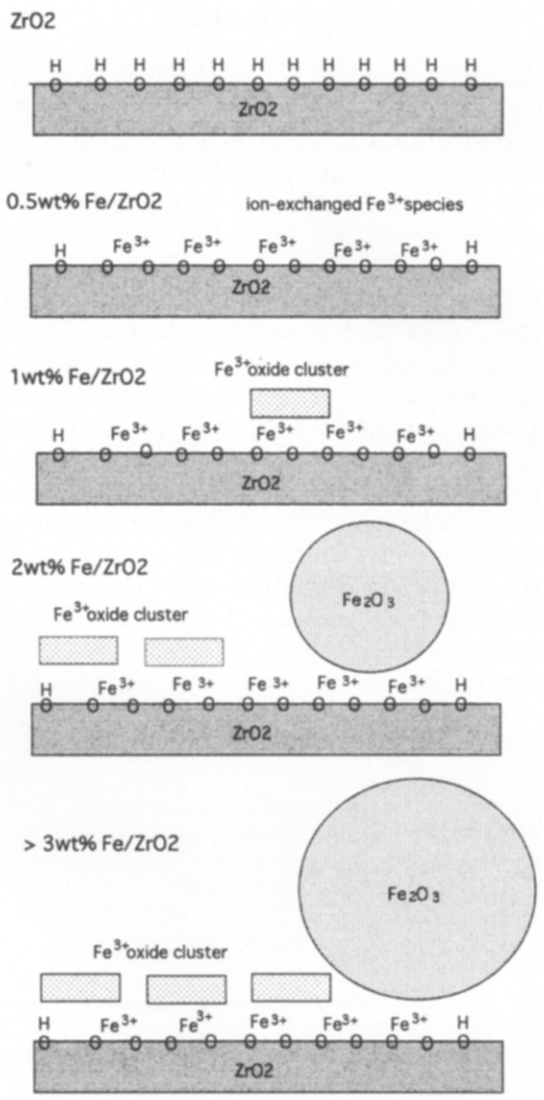

FIG. 15. Schematic model of Fe/ZrO_2 calcined at 973 K as a function of Fe loading.

The addition of a small amount of Cu significantly improves the catalytic activity of Fe/ZrO_2 for the NO–CO reaction. The Mössbauer results indicate a considerable increase in the dispersion of Fe^{3+} species to form the maximum amount of highly dispersed Fe^{3+} species (1.44 wt% Fe), although the causes are not clear at the moment. However, the activity increase by more than 10 times on the addition of Cu cannot be explained merely by the increase in the catalytically active phase. The synergistic effect of Cu could be ascribed to cooperative involvement of both Fe and Cu species in the reaction as evidenced by the change in the rate equation. In the previous study (14) using Cu K-edge XAFS, we have suggested the formation of Cu–O–Fe bonds in Cu/ZrO_2 promoted by Fe.

With Fe/Al_2O_3 and Fe/SiO_2 catalysts calcined at 973 K, the catalytic activities are significantly lower than that for Fe/ZrO_2 at a low Fe loading. As discussed by other workers (26, 32), the Mössbauer results indicate the preferential formation of Fe^{3+} paramagnetic species, such as small $FeAlO_3$ particles (43), at 5 wt% Fe caused by dissolution of Fe^{3+} cations into the subsurface and/or bulk phases. In conformity with this, a slightly higher Fe $2p_{3/2}$ binding energy is observed for 5 wt% Fe/Al_2O_3 than for Fe_2O_3. In the case of 5 wt% Fe/SiO_2, no surface Fe species were detected in the present XPS study. The formation of the binary oxide phases is confirmed for 5 wt% Fe/Al_2O_3 and Fe/SiO_2 by the EXAFS results in Fig. 10 and Table 3. At a high Fe loading (20 wt% Fe), a considerable fraction of the surface Fe species in Fe/Al_2O_3 is composed of Fe_2O_3 particles, which show moderate activity for the NO–CO reaction.

5. CONCLUSIONS

In the present study, it is revealed that Fe/ZrO_2 shows very high activity for the NO–CO reaction at 523 K at a low Fe content (5 wt% Fe). Characterization of Fe/ZrO_2 with various Fe contents by ^{57}Fe Mössbauer spectroscopy, IR, XRD, XPS, and EXAFS leads us to conclude that three kinds of Fe^{3+} species are formed on Fe/ZrO_2 calcined at 973 K: Fe^{3+} cation species preferentially produced at a low Fe content by ion-exchange with the surface OH groups of ZrO_2, Fe^{3+} oxide clusters much smaller than 8 nm in size, and large α-Fe_2O_3 particles (>27 nm in diameter). The maximum amounts of the Fe^{3+} cation species and Fe^{3+} oxide clusters are 2.8 and 3.4 Fe nm^{-2}, respectively. It is shown that the Fe^{3+} oxide clusters are highly active for the NO–CO reaction at 523 K, whereas the Fe^{3+} cation species are almost inactive. The addition of 0.5 wt% Cu promotes the activity of Fe/ZrO_2 more the ten times. The catalytic synergy between Cu and Fe is attributed to cooperative involvement of both Cu and Fe in the reaction. The effect of the calcination temperature on the iron species of Fe/ZrO_2 will be reported elsewhere (44).

ACKNOWLEDGMENTS

The X-ray absorption measurements were performed under the approval of the Photon Factory (KEK-PF) Program Advisory Committee (Proposal 93G-163). We are grateful to Dr. S. Tsutsui (Japan Atomic Energy Research Institute) for useful discussions.

REFERENCES

1. Taylor, K. C., *in* "Catalysis-Science and Technology," Vol. 5, p. 119. Springer-Verlag, Berlin, 1984.
2. Iwamoto, M., Yahiro, H., Yu-u, Y., Shundo, S., and Mizuno, M., *Shokubai* **32**, 430 (1990).
3. Held, W., Koenig, A., Richter, T., and Pauppe, L., SAE Paper 900496, 1990.
4. Iwamoto, M., and Hamada, H., *Catal. Today* **10**, 57 (1991).
5. Iwamoto, M., and Yahiro, H., *Catal. Today* **22**, 5 (1994).
6. Funabiki, M., Yamada, T., and Kayano, K., *Catal. Today* **10**, 33 (1991).
7. Nakajima, F., *Catal. Today* **10**, 1 (1991).
8. Hamada, H., *Catal. Survey Jpn.* **1**, 53 (1997).
9. Shelef, M., Otto, K., and Gandhi, H., *J. Catal.* **12**, 361 (1968).
10. Okamoto, Y., Ohto, Y., and Imanaka, T., *Kagaku Kogaku Ronbunshu* **19**, 863 (1993).
11. Yamaguchi, T., Tanno, M., and Tanabe, K., *Stud. Surf. Sci. Catal.* **63**, 567 (1991).
12. Okamoto, Y., and Gotoh, H., *Catal. Today* **36**, 71 (1997).
13. Okamoto, Y., Gotoh, H., Aritani, H., Tanaka, T., and Yoshida, S., *J. Chem. Soc. Faraday Trans.* **93**, 3879 (1997).
14. Okamoto, Y., Kubota, T., Gotoh, H., Ohto, Y., Aritani, H., Tanaka, T., and Yoshida, S., *J. Chem. Soc. Faraday Trans.* **94**, 3743 (1998).
15. Mizuno, N., Yamamoto, M., Tanaka, M., and Misono, M., *Bull. Chem. Soc. Jpn.* **64**, 1383 (1991).
16. Mizuno, N., Yamamoto, M., Tanaka, M., and Misono, M., *J. Catal.* **132**, 560 (1991).
17. Mizuno, N., Fujii, H., Igarashi, H., and Misono, M., *J. Am. Chem. Soc.* **114**, 7151 (1992).
18. Hsu, C. Y., Heimbuch, C. R., Armes, C. T., and Gates, B. C., *J. Chem. Soc. Chem. Commun.* 1645 (1992).
19. Jatia, A., Chan, C., MacLeod, J. D., Okubo, T., and Davis, M. E., *Catal. Lett.* **25**, 21 (1994).
20. Wan, K. T., Khouw, C. B., and Davis, M. E., *J. Catal.* **158**, 311 (1996).
21. Cheung, T. K., and Gates, B. C., *Topics Catal.* **6**, 41 (1998).
22. Yamaguchi, T., *Catal. Today* **20**, 199 (1994).
23. Ji, W., Kuo, Y., Shen, S., Li, S., and Wan, H., *in* "Proceedings, 10th International Congress on Catalysis, Budapest, 1992" (L. Guczi, F. Solymosi, and P. Tetenyi, Eds.), p. 2059. Akadémiai Kiadó, Budapest, 1993.
24. Yamamoto, T., Tanaka, T., Takenaka, S., Yoshida, S., Onari, T., Takahashi, Y., Kosaka, T., Hasegawa, S., and Kudo, M., *J. Phys. Chem. B* **103**, 2385 (1999).
25. Chen, K., Fan, Y., Hu, Z., and Yan, Q., *Catal. Lett.* **36**, 139 (1996).
26. Chen, K., Dong, L., Yan, Q., and Chen, Y., *J. Chem. Soc. Faraday Trans.* **93**, 2203 (1997).
27. Murakami, Y., *in* "Preparation of Catalysts III" (G. Poncelet, P. Grange, and P. A. Jacobs, Eds.), p. 775. Elsevier, Amsterdam, 1983.
28. Nasu, S., and Shimizu, S., *J. Catal.* **104**, 164 (1987).
29. Rehr, J. J., Mustre de Leon, J., Zabinsky, S. I., and Albers, R. C., *J. Am. Chem. Soc.* **113**, 5135 (1991).
30. Gallezot, P., *in* "Catalysis–Science and Technology" (J. R. Anderson and M. Boudart, Eds.), Vol. 5, p. 221. Springer-Verlag, Berlin, 1984.
31. Delgass, W. N., and Boudart, M., *Catal. Rev. Sci. Eng.* **2**, 129 (1968).
32. Gager, H. M., and Hobson, M. C., Jr., *Catal. Rev. Sci. Eng.* **11**, 17 (1975).
33. Delgass, W. N., Haller, G. L., Kellerman, R., and Lunsford, J. H., "Spectroscopy in Heterogeneous Catalysis," p. 132. Academic Press, New York, 1979.
34. Niemantsverdriet, J. W., "Spectroscopy in Catalysis," p. 111. VCH, Weinheim, 1995.
35. Ying, Y., Li, Z., and Hu, J., *Sci. China Ser. B* **25**, 989 (1982).
36. Kerkhof, F. P. J. M., and Moulijn, J. M., *J. Phys. Chem.* **83**, 1612 (1979).
37. Delgass, W. N., Haller, G. L., Kellerman, R., and Lunsford, J. H., "Spectroscopy in Heterogeneous Catalysis," p. 267. Academic Press, New York, 1979.
38. Niemantsverdriet, J. W., "Spectroscopy in Catalysis," p. 37. VCH, Weinheim, 1995.
39. Antipin, M. Y., Tzirelson, V. G., Flugge, M. P., Gerr, R. G., Struchkov, Y. T., and Ozerov, R. P., *Dokl. Acad. Nauk.* **281**, 854 (1985).
40. Yamaguchi, T., Nakano, Y., and Tanabe, K., *Bull. Chem. Soc. Jpn.* **51**, 3482 (1978).
41. Kündig, W., Bömmel, H., Constabaris, G., and Lindquist, R. H., *Phys. Rev.* **142**, 327 (1966).
42. Ganguly, B., Huggins, F. E., Rao, K. R. P. M., and Huffman, G. P., *J. Catal.* **142**, 552 (1993).
43. Chernavskii, P. A., and Lunin, V. V., *Kinet. Catal.* **34**, 470 (1993).
44. Okamoto, Y., Kubota, T., Ohto, Y., and Nasu, S., submitted.